Continental J. Applied Sciences
Ojemeri et al. (2023) 18 (1): 18 – 40 Doi: 10.5281/zenodo.7932942

Research Article

Arrhenius-Controlled Heat Transfer Fluid Provoked by Porosity Effect through a Vertical Micro-Channel: An Analytical Approach

Godwin Ojemeri[1]* Isaac O. Onwubuya[2] Abdulsalam Shuaibu[3], Emmanuel Omokhuale[4], Mohammad M. Altine[5]
[1,3] Department of Mathematics, College of Sciences, Federal University of Agriculture, P. M. B. 28, Zuru, Kebbi State, Nigeria.
[2]Department of Mathematics, Faculty of Sciences, Air Force Institute of Technology, P. M. B. 2104, Kaduna State, Nigeria.
[4]Department of Mathematics, Faculty of Sciences, Federal University Gusau, P. M. B 1001, Zamfara State.
[5]Department of Mathematics, Federal University, Birnin Kebbi, P. M. B. 1157, Kebbi State, Nigeria.
*Corresponding Author's email: godwinojemeri@gmail.com

Abstract

This article basically focuses on the analytical treatment of Arrhenius-controlled fluid in a vertical micro-channel saturated with porous material. The leading equations are solved in dimensionless form using the homotopy perturbation method (HPM) subject to relevant boundary conditions. The fundamental flow features of temperature, velocity, and volume flow rate is investigated as a function of controlling parameters such as chemical reaction parameters, rarefaction parameter, fluid-wall interaction parameter, wall-ambient temperature difference ratio, and Darcy number. The findings are thoroughly investigated and graphically represented in a number of illustrative plots. It is worth noting that the variations of chemical reaction, Darcy number, rarefaction and wall-ambient temperature difference ratio parameters substantially dictate the fluid flow and volume flow rate respectively.

KEYWORDS: Homotopy perturbation method, Arrhenius kinetics, rarefaction, porosity effect, wall ambient temperature ratio, Micro-channel

Received: 21 March 2023 Accepted: 11 May 2023

ISSN: 1597 – 9928. Science and Education Development Inst., Nigeria

Nomenclature

B_0 =constant magnetic flux density
g=gravitational acceleration
b= channel width
$C_p C_v$=specific heats at constant pressure and constant volume respectively
In=fluid -wall interaction parameter
Kn =Knudsen number a/b
Ka=Darcy number
λ=chemical reactant parameter
Q=dimensionless volume flow rate
M= Hartmann number
Pr=Prandtl number
Nu=dimensionless heat transfer rate
e=activation energy
T=temperature of the fluid
T_0=reference temperature
u=velocity component in x direction
U=dimensionless velocity

Greek letters

β =thermal expansion coefficient
$\beta_t \beta_v$ =dimensionless variables
μ =dynamic viscosity
α =thermal diffusivity
γ_s = ratios of specific heats ($C_p C_v$)
ξ =wall-ambient temperature difference ratio
σ =electrical conductivity of the fluid
ρ = density
v=fluid kinematic viscosity

Introduction

Micro-channel fluid and heat transfer flows have gained popularity in recent years due to their vast range of cooling applications in material processing operations and manufacturing, micro heat pipe, space systems, micro-channel heat absorption, micro-jet impingement cooling, high power density chips in supercomputers, and other electronics. Because the majority of these designs include inward micro-channel flows, understanding the flow pattern are becoming increasingly important for proper and

ISSN: 1597 – 9928. Science and Education Development Inst., Nigeria

accurate modeling predictions and formulation (Al-Nimr and Khadrawi, 2004, Jha et al. 2014a). Several recent researches have been presented to analyze the impact of fluid flows on micro geometry in a variety of physical settings. Jha and Malgwi (2019a) investigated the combined effect of Hall current and the ion-slip condition on magneto-hydrodynamics (MHD) natural convection flow in a vertical micro-channel under the influence of an induced magnetic field. Jha and Aina (2016) later solved MHD free convection in a vertical micro-channel built from two electrically non-conducting infinite vertical parallel plates with great precision. As part of their research, Jha et al. (2017) investigated the effect of Hall current on MHD natural convection flow in a vertical micro-channel. Other works in this area include (Chen and Weng 2005, Jha and Aina 2015, Buonomo and Manca 2012, Weng and Chen 2009, Jha et al. 2014b) to cite a few.

In recent decades, engineers and scientists have been intrigued by the study of the electrically conducting fluid phenomenon, simply called magneto-hydrodynamics (MHD), due to its importance in many MHD applications like MHD generators, electric transformers, cooling of metallic plates in cooling baths, and MHD accelerators, among others. (MHD) pumps are already used in chemical energy technology to pump electrically conducting fluids in several atomic energy centers. Aside from these uses, when the fluid is electrically conducting, an applied magnetic field can significantly accelerate natural convection flow (Jha *et al*. 2015). Several studies of MHD convective flow in various physical settings have been carried out. In light of this, Ojemeri et al. (2023) recently investigated the steady state MHD-free flow of a Casson fluid that is electrically conductive and controlled by thermal radiation effect in a vertical porous channel. Gul et al. (2021) investigated the hybrid Nanofluid influence on MHD boundary surface flow for viscous fluids. Saeed and Gul (2021) emphasized the MHD Casson Nanofluid flow for heat and mass transfer towards a moving plate. Aziz and Shams (2020) investigated the emission of entropy for the MHD Maxwell nanofluid flow under the slip effect, thermal radiation, heat emission and varying thermal conductivity. Gurivireddy *et al*. (2016) simulated the impacts of heat production and chemical reactions on MHD flow using a semi-infinite moving vertical porous plate with thermal diffusion. Other literatures cited include (Sheikholeslamia and Gorji-Bandpy 2014, Ali *et al*. 2012).

The formulation of flow models through viscous or chemically reactive fluids with MHD free and mixed convection contemplated by different geometrical surfaces has attracted growing interest over the years due to its interesting and possible applications in transpiration cooling of re-entry vehicles and rocket boosters, film vaporization in combustion chambers, and cross-hatching on ablative surfaces (Muthuraj and Srinivas 2010). The modeling of reactive viscous fluids was first presented by Frank–Kamenetskii (1969). According to Makinde (2008), most lubricants used in engineering and industrial processes, such as synthetic esters, hydrocarbon oils, polyglycols, and so on, are reactive. Quite recently, in light of these considerations, Hamza *et al.* (2023) recently published a theoretical study on the effect of Arrhenius-controlled heat transfer flow influenced by an induced magnetic field in a microchannel. Ojemeri and Hamza (2022) put forth a theoretical investigation of heat generating/absorbing fluid controlled by Arrhenius kinetic in a microchannel. Hamza *et al.* (2019) offered an analytical study on the effects of radial magnetic field flow of chemically reactive fluid in a vertical porous annulus in the existence of mixed convection and soret effects. Ojemeri et al. (2019) searched the slip and Soret effects of the free convection flow of a viscous, reactive fluid through a vertical porous cylinder with a radial magnetic field. Ahmad and Jha (2015) presented the steady and unsteady influence of the fully developed free heat transfer flow of reactive viscous fluids in a vertical porous pipe. They concluded that the time-dependent and steady-state rates of heat transmission through pipe layers increased with time. Jha et al. (2011a, 2011b) proposed a reactive viscous flow in an unsteady free convection flow in a vertical channel and a tube. According to their calculations, higher values of the reactant consumption parameter contribute to an increase in heat transfer rate and friction factor on both channel walls. Hamza (2016) discussed the unsteady/steady free convection flow of a chemically reacting fluid in a vertical channel, taking into account the velocity slip conditions and Newtonian heating.

The use of porous media in micro-channels and heat exchangers is a technique that is becoming more and more intriguing for enhancing convection heat transfer characteristics. A porous medium, according to Mahmoudi *et al.* (2020), is a solid matrix with void spaces called pores that are linked by a system of channels through which fluid can flow. Numerous applications such as the storage of radioactive nuclear waste, geothermal extraction, transpiration cooling, filtration, crude oil extraction, heating and cooling in buildings, and many others, involve the flow of fluid and the transmission of heat within channels saturated with porous medium. Using Hamming's predictor-corrector approach, Joshi and Gebhart (1985) offered a technical remark on the mixed-convection mechanism through a heat flux surface with a porous material. In order to get numerical results with free-stream velocity and modest amplitude fluctuations in the wall temperature embedded in a porous material, Chamkha (2007) used the Kellerbox technique. Chamkha *et al*. (2011) analyzed the action of a transverse magnetic field on mixed-convection events over a semi-infinite permeable vertical plate in a porous medium with uniform heat flux. The MHD convection flow of Casson fluid in micro-channels including porous material was discussed by Gireesha and Sindhu (2020). When Alam *et al*. (2021) used network simulation method solutions to analyze time-dependent hydro-magnetic radiative fluid flow over an inclined porous plate with heat and mass permeability, they found that the fluid momentum tended to rise or fall gradually

ISSN: 1597 – 9928. Science and Education Development Inst., Nigeria

towards the plate and then diminish or grow slowly away from the plate. The temperature of the fluid has been reported to exhibit the same tendency.

The objective of this current study is to extend the work of Jha *et al.* (2014a) by using the homotopy perturbation approach to scrutinize the consequences of chemical reactant parameter having porous material on fully developed steady free convection flow in a vertical micro-channel. The novelty of this investigation is that an approximate solution for the flow of chemically reacting, viscous, and electrically conducting fluid controlled by Arrhenius kinetics within two vertical micro-channel walls saturated with porous medium was obtained using HPM. Results obtained from this research can be impactful in a wide spectrum of possible applications, such as micro-devices based on micro-fabrication techniques, micro-electro-mechanical systems (MEMS), biomedical engineering, transpiration cooling, geothermal extraction, the storage of radioactive nuclear waste, and a variety of medical treatment methods, especially in the thermal therapeutic process.

Problem formulation

The steady, fully developed free convection flow of a chemically reacting fluid in a vertical micro-channel confined by two electrically non-conducting infinite vertical parallel plates is considered under the effect of Darcy number. The x-axis is perpendicular to but opposite the gravitational acceleration g, while the y-axis is orthogonal to the vertical plate. The flow arrangement and coordinate system for this flow problem are depicted in Figure 1. A uniform magnetic field of intensity B_0 is thought to be introduced in the direction perpendicular to the flow direction. It is also thought that the magnetic Reynolds number is very low, implying that the generated magnetic field is minimal in comparison to the one applied outwardly. The plates are heated asymmetrically, with one plate kept at T_1 and the other at T_2, with $T_1 > T_2$. Natural convection flow in the channel is caused by the temperature difference between the plates.

ISSN: 1597 – 9928. Science and Education Development Inst., Nigeria

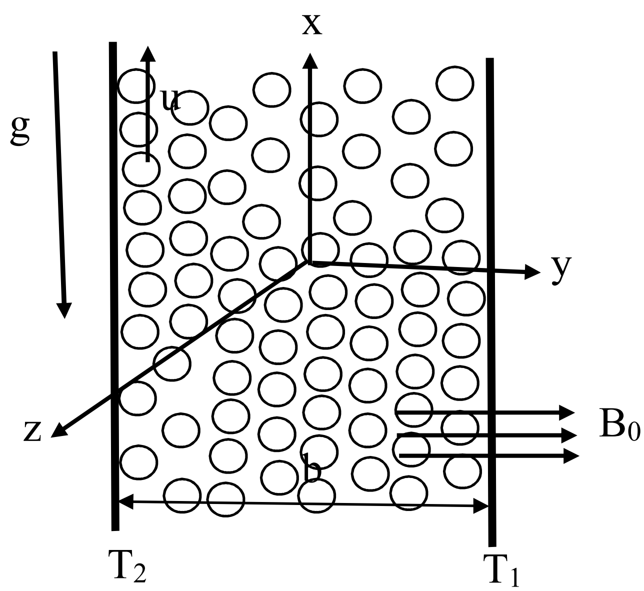

Figure 1: The physical coordinate of the flow system

Under the basic premise of the Boussinesq's approximation, the velocity and energy equations for the current problem are given in dimensionless form, following Jha *et al*. (2014a) and taking Darcy number and chemically reactive parameter into account.

$$\frac{d^2U}{dy^2} - (M^2 + \frac{1}{Ka})U = -\theta \tag{1}$$

$$\frac{d^2\theta}{dy^2} + \lambda e^{\frac{\theta}{1+\varepsilon\theta}} = 0 \tag{2}$$

The boundary conditions at the wall surfaces are as follows;

$$\left.\begin{array}{llll} U(Y) = \beta_v Kn\dfrac{dU}{dy}, & \theta(Y) = \xi + \beta_v KnIn\dfrac{d\theta}{dy}, & at & y = 0 \\ U(Y) = -\beta_v Kn\dfrac{dU}{dy}, & \theta(Y) = 1 - \beta_v KnIn\dfrac{d\theta}{dy}, & at & y = 1 \end{array}\right\} \tag{3}$$

Where the dimensional quantities used in the flow problem are given below as follows:

$$\beta_v = \frac{2-f_v}{f_v}, \quad \beta_t = \frac{2-f_t}{f_t}\frac{2\gamma_s}{\gamma_s+1}\frac{1}{\Pr}, \quad Kn = \frac{a}{b}, \quad In = \frac{\beta_t}{\beta_v}, \quad \xi = \frac{T_2 - T_0}{T_1 - T_0}$$

$$Y = \frac{y}{b}, \; \theta = \frac{T-T_0}{T_1-T_0}, \quad U = \frac{u}{U_0}, \quad M^2 = \frac{\sigma B_0^2 b^2}{\rho v}, \; \Pr = \frac{v}{\alpha}, \quad where\;\; U_0 = \frac{\rho g \beta (T_1 - T_0) b^2}{\mu}$$

$$\varepsilon = \frac{RT_0}{E}, \quad \lambda = \frac{QC_0^* AEH^2}{RT_0^2} e^{(\frac{-E}{RT_0})}, \; Ka = \frac{\kappa}{h^2}$$

The dimensionless quantities used in the equations are defined in the nomenclature.

Methodology

Closed form solution

We employed the homotopy perturbation method to solve the governing equations, constructing a convex homotopy on equations (1) and (2) to get:

$$H(U,p) = (1-p)\frac{d^2U}{dy^2} - p\left[(M^2 + \frac{1}{Ka})U - \theta\right] = 0 \tag{4}$$

$$H(\theta,p) = (1-p)\frac{d^2\theta}{dy^2} + p\left[\lambda e^{\frac{\theta}{1+\varepsilon\theta}}\right] = 0 \tag{5}$$

Assuming the solutions of U and θ to be in an infinite series form as follows:

$$\left.\begin{aligned} \theta(Y) &= \theta_0 + p\theta_1 + p^2\theta_2 + \ldots \\ U(Y) &= u_0 + pu_1 + p^2u_2 + \ldots \end{aligned}\right\} \tag{6}$$

and substituting equation (6) into equations (4) and (5), and comparing the coefficient of like powers p, we have the following sets of differential equations with their corresponding transformed boundary conditions as follows:

$$p^0 : \begin{cases} \dfrac{d^2\theta_0}{dy^2} = 0 & (7) \\[2ex] \dfrac{d^2u_0}{dy^2} = 0 & (8) \end{cases}$$

The corresponding transformed boundary conditions now becomes

$$\left.\begin{aligned}\theta_0 &= \xi + \beta_v KnIn\frac{d\theta_0}{dy}\\ u_0 &= \beta_v Kn\frac{du_0}{dy}\end{aligned}\right\} \quad at \quad y=0 \tag{9}$$

$$\left.\begin{aligned}\theta_0 &= 1 - \beta_v KnIn\frac{d\theta_0}{dy}\\ u_0 &= -\beta_v Kn\frac{du_0}{dy}\end{aligned}\right\} \quad at \quad y=1 \tag{10}$$

$$p^1 : \begin{cases} \dfrac{d^2\theta_1}{dy^2} + \lambda(1+\theta_0+\left(2-\varepsilon\right)\theta_0^2) = 0 & (11)\\ \dfrac{d^2u_1}{dy^2} - (M^2+\dfrac{1}{Ka})u_0 + \theta_0 = 0 & (12)\end{cases}$$

The transformed boundary conditions now become

$$\left.\begin{aligned}\theta_1 &= \beta_v KnIn\frac{d\theta_1}{dy}\\ u_1 &= \beta_v Kn\frac{du_1}{dy}\end{aligned}\right\} \quad at \quad y=0 \tag{13}$$

$$\left.\begin{aligned}\theta_1 &= -\beta_v KnIn\frac{d\theta_1}{dy}\\ u_1 &= -\beta_v Kn\frac{du_1}{dy}\end{aligned}\right\} \quad at \quad y=1 \tag{14}$$

$$p^2 : \begin{cases} \dfrac{d^2\theta_2}{dy^2} + \lambda(\theta_1 - 2\varepsilon\theta_1\theta_0 + 4\theta_1\theta_0) = 0 & (15)\\ \dfrac{d^2u_2}{dy^2} - (M^2+\dfrac{1}{Ka})u_1 + \theta_1 = 0 & (16)\end{cases}$$

ISSN: 1597 – 9928. Science and Education Development Inst., Nigeria

The transformed boundary conditions now become

$$\left.\begin{aligned}\theta_2 &= \beta_v KnIn\frac{d\theta_2}{dy} \\ u_2 &= \beta_v Kn\frac{du_2}{dy}\end{aligned}\right\} \quad at \quad y=0 \tag{17}$$

$$\left.\begin{aligned}\theta_2 &= -\beta_v KnIn\frac{d\theta_2}{dy} \\ u_2 &= -\beta_v Kn\frac{du_2}{dy}\end{aligned}\right\} \quad at \quad y=1 \tag{18}$$

Setting p=1, the solutions of the differential equations in the approximate form becomes

$$\left.\begin{aligned}\theta &= \lim_{p\to 1}\theta = \theta_0+\theta_1+\theta_2+\dots \\ U &= \lim_{p\to 1}U = u_0+u_1+u_2+\dots\end{aligned}\right\} \tag{19}$$

In most cases, the series (19) converges even for a few terms. The nonlinear operator, on the other hand, determines the rate of convergence. According to Ayati and Biazar (2015), the homotopy perturbation converges on the series solution, revealing that only a few terms of the HPM series can be used to obtain an approximate solution.

The solutions of $\theta_0, \theta_1, \theta_2 \dots \quad and \quad u_0, u_1, u_2 \dots$ is as follows:

$$\theta_0 = A_0 + A_1 y \tag{20}$$

$$\theta_1 = -\lambda\left[\ \frac{y^2}{2} + A_0\frac{y^2}{2} + A_1\frac{y^3}{6} + (2-\varepsilon)(A_0^2\frac{y^2}{2} + A_0A_1\frac{y^3}{3} + A_1^2\frac{y^4}{12})\ \right] + A_3 y + A_2 \tag{21}$$

$$\begin{aligned}\theta_2 = -(4\lambda - 2\varepsilon\lambda)\Bigg[&\lambda\left\{A_0\frac{y^4}{24} + A_0^2\frac{y^4}{24} + A_0A_1\frac{y^5}{120} + (2-\varepsilon)(A_0^3\frac{y^4}{24} + A_0^2A_1\frac{y^5}{60} + A_0A_1^2\frac{y^6}{360})\ \right\} \\ &+A_0A_3\frac{y^3}{6} + A_0A_2\frac{y^2}{2} - \lambda\left\{A_1\frac{y^5}{40} + A_0A_1\frac{y^5}{40} + A_1^2\frac{y^6}{180} + (2-\varepsilon)(A_0^2A_1\frac{y^5}{40} + A_0A_1^2\frac{y^6}{60} + A_1^3\frac{y^7}{504})\ \right\} \\ &+A_3A_1\frac{y^4}{12} + A_2A_1\frac{y^3}{6}\ \Bigg] + \lambda^2\left\{\frac{y^4}{24} + A_0\frac{y^4}{24} + A_1\frac{y^5}{120} + (2-\varepsilon)(A_0^2\frac{y^4}{24} + A_0A_1\frac{y^5}{60} + A_1^2\frac{y^6}{360})\ \right\} \\ &+\lambda(A_3\frac{y^3}{6} + A_2\frac{y^2}{2}) + A_5 y + A_4\end{aligned} \tag{22}$$

ISSN: 1597 – 9928. Science and Education Development Inst., Nigeria

$$u_1 = -A_0\frac{y^2}{2} - A_1\frac{y^3}{6} + D_3 y + D_2 \tag{23}$$

$$u_2 = (M^2 + \frac{1}{Ka})(-A_0\frac{y^4}{24} - A_1\frac{y^5}{120} + D_3\frac{y^3}{6} + D_2\frac{y^2}{2}) + \lambda\Big\{\frac{y^4}{24} + A_0\frac{y^4}{24} + A_1\frac{y^5}{120}$$
$$+(2-\varepsilon)(A_0^2\frac{y^4}{24} + A_0A_1\frac{y^5}{60} + A_1^2\frac{y^6}{360})\ \Big\} - A_3\frac{y^3}{6} - A_2\frac{y^2}{2} + D_5 y + D_4 \tag{24}$$

Equations (20) – (24) gives the expressions for the energy and momentum as
$\theta(Y) = \theta_0 + \theta_1 + \theta_2 + \ldots$
$U(Y) = u_0 + u_1 + u_2 + \ldots$

Volume flow rate and heat transfer amount are two critical parameters for buoyancy-induced micro flow and micro heat transfer, respectively. The dimensionless volume flow rate can be calculated using the following formula:

$$Q_m = \int_0^1 U dY \tag{25}$$

$$Q_m = -\frac{A_0}{6} - \frac{A_1}{24} + \frac{D_3}{2} + D_2 + (M^2 + \frac{1}{Ka})(-\frac{A_0}{120} - \frac{A_1}{720} + \frac{D_3}{24} + \frac{D_2}{6}) + \lambda\Big[\frac{1}{120} + \frac{A_0}{120} + \frac{A_1}{720}$$
$$(2-\varepsilon)(\frac{A_0^2}{120} + \frac{A_0A_1}{360} + \frac{A_1^2}{2520})\ \Big] - \frac{A_3}{24} - \frac{A_2}{6} + \frac{D_5}{2} + D_4 \tag{26}$$

And the rate of heat transfer at both plates are given as

$$Nu_0 = \frac{qb}{(T_1 - T_0)k} = \frac{d\theta}{dy}\Big|_{y=0} = A_1 + A_3 + A_5 \tag{27}$$

$$Nu_1 = \frac{qb}{(T_1 - T_0)k} = \frac{d\theta}{dy}\Big|_{y=1} = A_1 - \lambda\Big[1 + A_0 + \frac{A_1}{2} + (2-\varepsilon)(A_0^2 + A_0A_1 + \frac{A_1^2}{3})\Big] + A_3 - (4\lambda - 2\varepsilon\lambda)\Big[\frac{A_0}{6} + \frac{A_0^2}{6} + \frac{A_0A_1}{24}$$
$$(2-\varepsilon)(\frac{A_0^3}{6} + \frac{A_0^2A_1}{12} + \frac{A_0A_1^2}{60}) + \frac{A_0A_3}{2} + A_0A_2 - \lambda\Big\{\frac{A_1}{8} + \frac{A_0A_1}{8} + \frac{A_1^2}{60}$$
$$+(2-\varepsilon)(\frac{A_0^2A_1}{8} + \frac{A_1^2A_0}{10} + \frac{A_1^3}{72})\ \Big\} + \frac{A_3A_1}{3} + \frac{A_0A_1}{2}\ \Big] + \lambda^2\Big\{\frac{1}{6} + \frac{A_0}{6} + \frac{A_1}{24} +$$
$$(2-\varepsilon)(\frac{A_0^2}{6} + \frac{A_0A_1}{12} + \frac{A_1^2}{60})\ \Big\} + \lambda(\frac{A_3}{2} + A_2) + A_5 \tag{28}$$

ISSN: 1597 – 9928. Science and Education Development Inst., Nigeria

We obtained the skin-friction (τ) on the plates as follows

$$sk\inf riction\left(\tau_0\right)=\left.\frac{dU}{dy}\right|_{y=0}=D_3+D_5 \tag{29}$$

$$sk\inf riction\left(\tau_1\right)=\left.\frac{dU}{dy}\right|_{y=1}=-A_0-\frac{A_1}{2}+D_3+(M^2+\frac{1}{Ka})(-\frac{A_0}{6}-\frac{A_1}{24}+\frac{D_3}{2}+D_2)+\lambda\left\{\frac{1}{6}+\frac{A_0}{6}+\frac{A_1}{24}\right.$$
$$\left.+(2-\varepsilon)(\frac{A_0^2}{6}+\frac{A_0A_1}{12}+\frac{A_1^2}{60})\ \right\}-\frac{A_3}{2}+A_2+D_5 \tag{30}$$

The constants used are all indicated in the appendix

Results and discussion

The effects of chemical reaction parameter (λ), Darcy number (Ka), wall-ambient temperature difference ratio (ξ), rarefaction parameter ($\beta_v Kn$) and fluid-wall interaction parameter (In) on a steady developed free convection and heat flow problem are discussed. The variation of temperature, velocity, volume flow rate, as well as some physical quantities of engineering interest such as skin-friction and rate of heat transfer are shown in Figures 2-10 and Tables 1-2 to illustrate the effects of these pertinent parameters. The current investigation was conducted in the continuum and slip flow regimes (Kn$\leq$0.1) over reasonable ranges of $0 \leq \beta_v Kn \leq 0.1$, and $0\leq In\leq 10$. The product of ($\beta_v Kn$) implies a measure of departure from the continuum regime, while (In) denotes a fluid-wall interaction feature. For this study, the chosen reference values for ($\beta_v Kn$) and (In) are 0.05 and 1.667, respectively, as presented by Chen and Weng (2005), and M=2 as presented by Jha *et al*. (2014a). Furthermore, the default values used in this study are λ =0.01, K=0.1 and ε =0.01 to evaluate the effects of different flow behaviors.

Figures 2 and 3 show the impacts of (λ) and (ξ) on the temperature and velocity gradients respectively under three cases of the wall-ambient temperature difference ratio (ξ =-1: one heating and one cooling; ξ =0: one heating and one not heating, ξ =1: both walls are heated). It is abundantly clear that as the value of (λ) increases, a large increase in the temperature jump is observed. In the same vein, It has been discovered that as the value of (λ) grows, the flow motion improves. Furthermore, it is determined that as velocity slip increases at the micro-channel wall, the fluid wall effect decreases, resulting in a rise in the gas velocity near the wall.

ISSN: 1597 – 9928. Science and Education Development Inst., Nigeria

Figures 4 and 5 describe the actions of rarefaction parameter (BvKn) on the temperature and velocity distributions respectively. A close look at these figures revealed that, as BvKn levels are raised, the velocity slip at the wall improves, which causes a retarding effect at the walls. This effect yields a noticeable increase in the gas velocity near the wall. In addition, increasing BvKn parameter makes the temperature to jump significantly and reduces the amount of heat transfer from the wall to the fluid.

Figure 6 describes the impact of Darcy number on the velocity. It is observed from the figure that the velocity increases with increasing Ka. This is physically true, when fluid material moved in quantity, more viscous energy is exhibited which yields an increase in the fluid boundary layer and thickness, consequently leading to a rise in the fluid velocity

The effects of (λ) and Darcy number on the volume flow are depicted in Figures 7 and 8. It is interesting to report that greater values of (λ) and Darcy number contributes to a pronounced increase in the volume flow rate. It is however worthy of note that the action of darcy number on the asymmetric case (ξ = -1) is seen to be insignificant

For different ascending values of (ξ), figures 9 and 10 demonstrate the variation of skin friction against ($\beta_v Kn$) parameter for (λ) and Darcy number at both micro-channel plates. As seen in figure 9, a rise in the chemical reactant parameter increases frictional force at y = 0 while the converse is observed at y = 1. A similar trend is observed in figure 10 when Darcy number is increased.

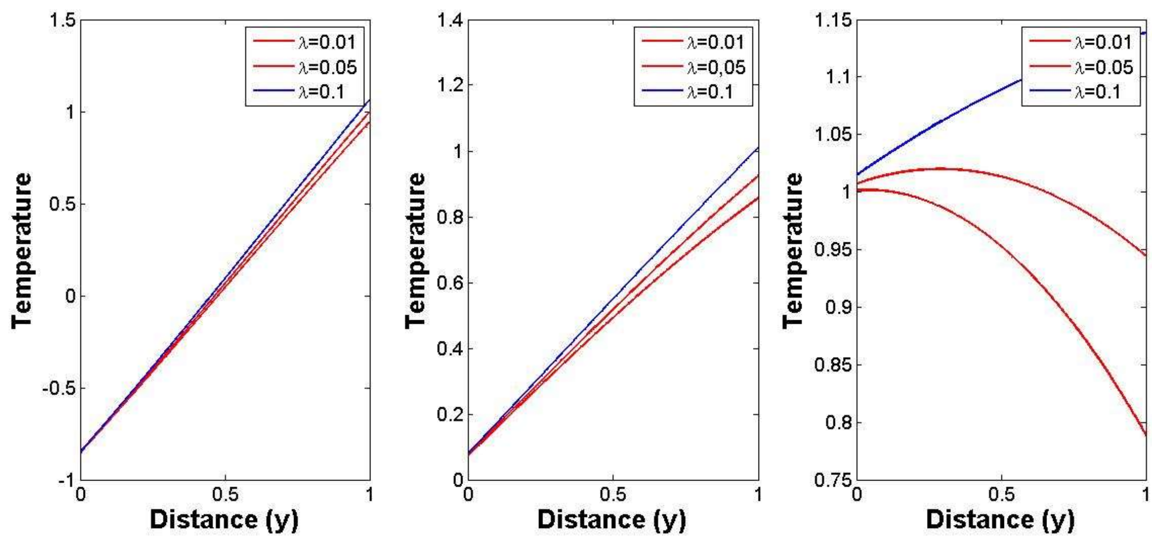

Figure 2: Temperature gradient for λ at (a) ξ=-1, (b) ξ=0 and (c) ξ=1

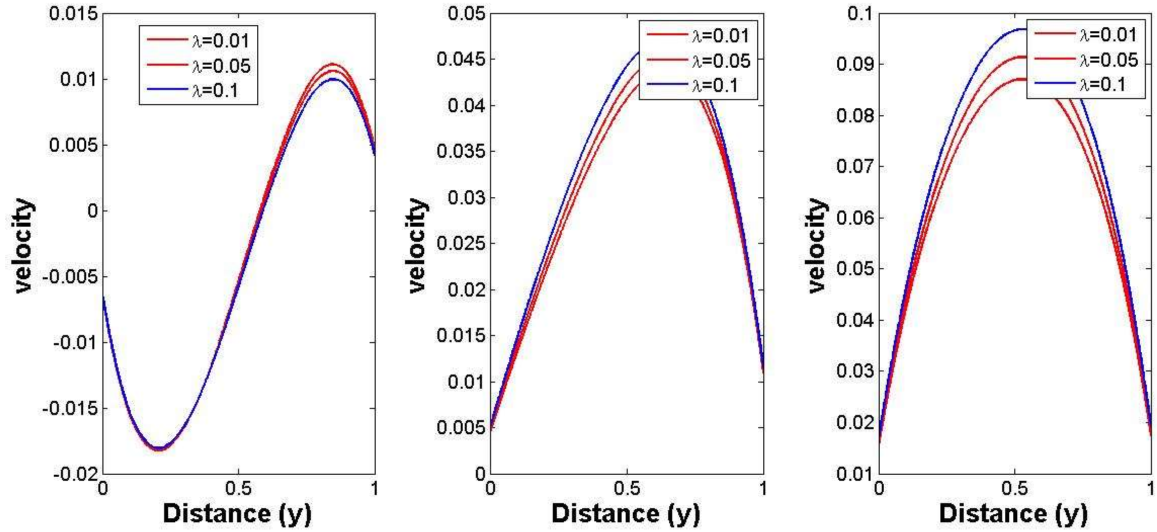

Figure 3: Velocity gradient for λ at (a) ξ=-1, (b) ξ=0 and (c) ξ=1

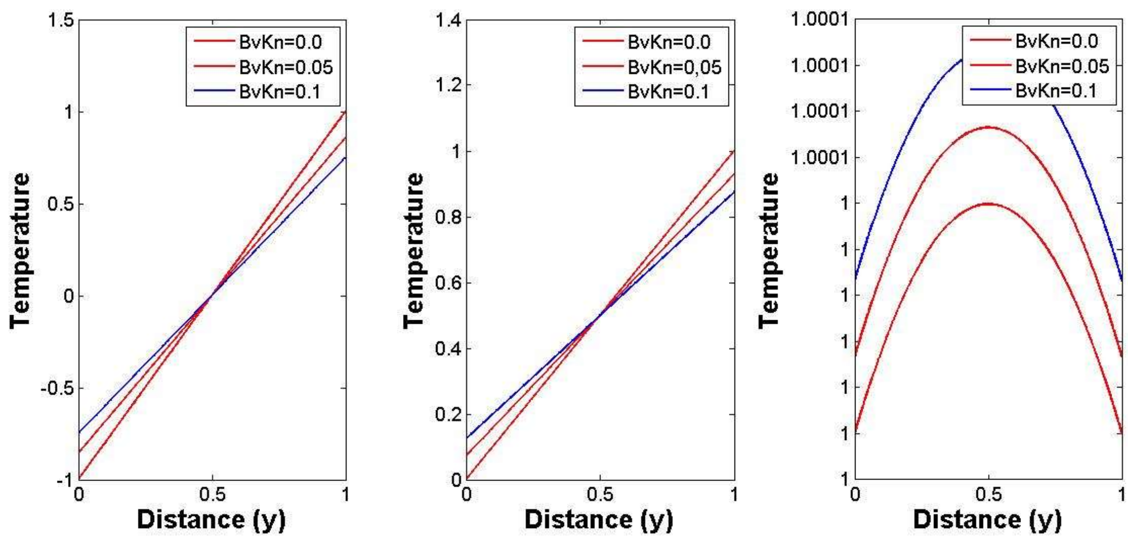

Figure 4: $\beta_v Kn$ on the temperature profile at (a) ξ=-1, (b) ξ=0 and (c) ξ=1

ISSN: 1597 – 9928. Science and Education Development Inst., Nigeria

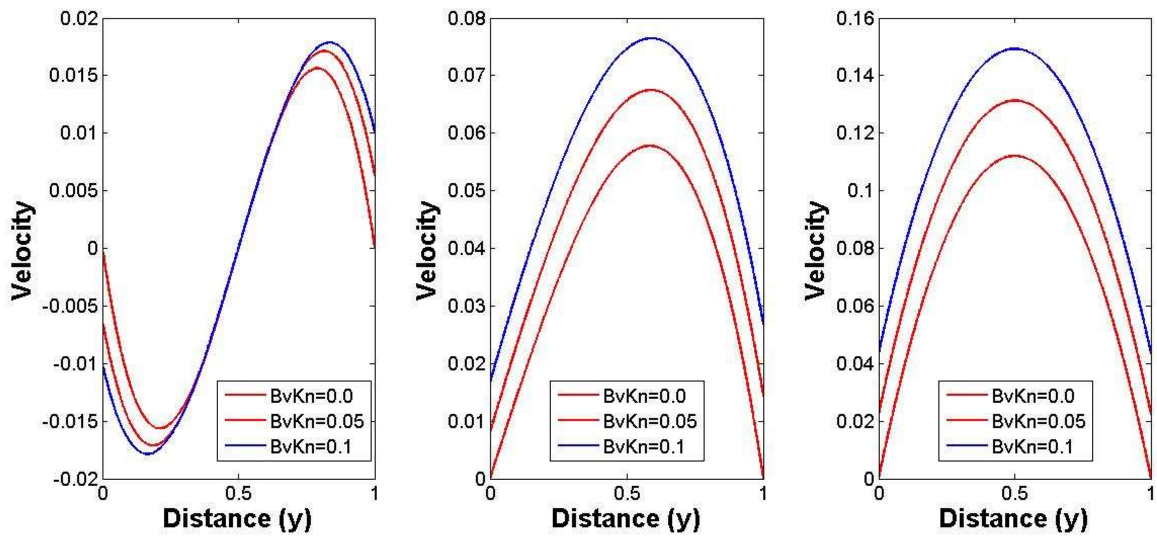

Figure 5: $\beta_v Kn$ on the velocity profile at (a) ξ=-1, (b) ξ=0 and (c) ξ=1

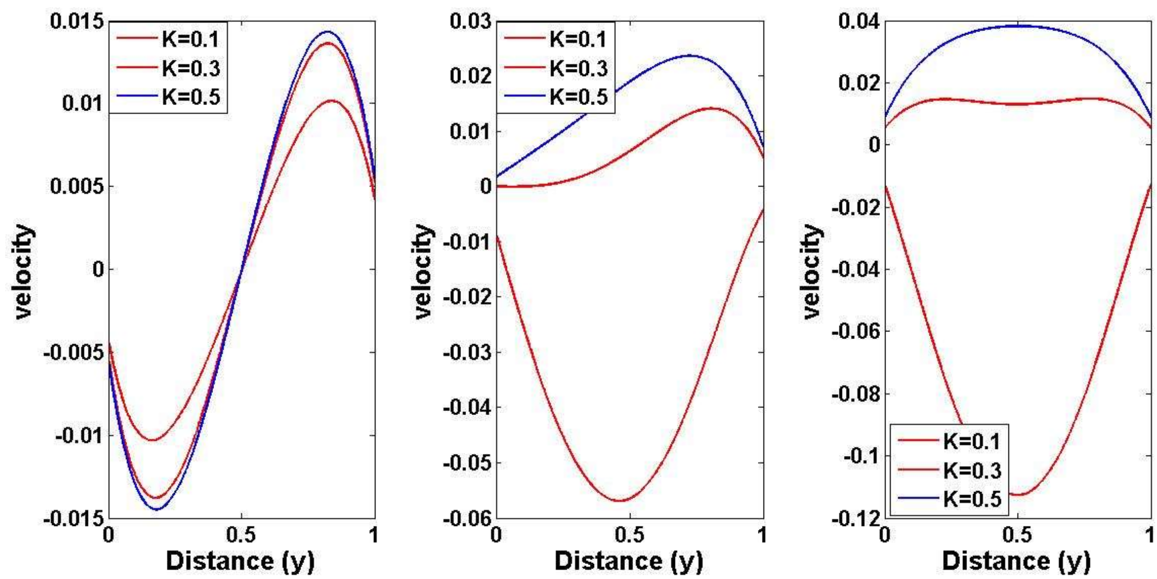

Figure 6: Ka on the velocity profile at (a) ξ=-1, (b) ξ=0 and (c) ξ=1

ISSN: 1597 – 9928. Science and Education Development Inst., Nigeria

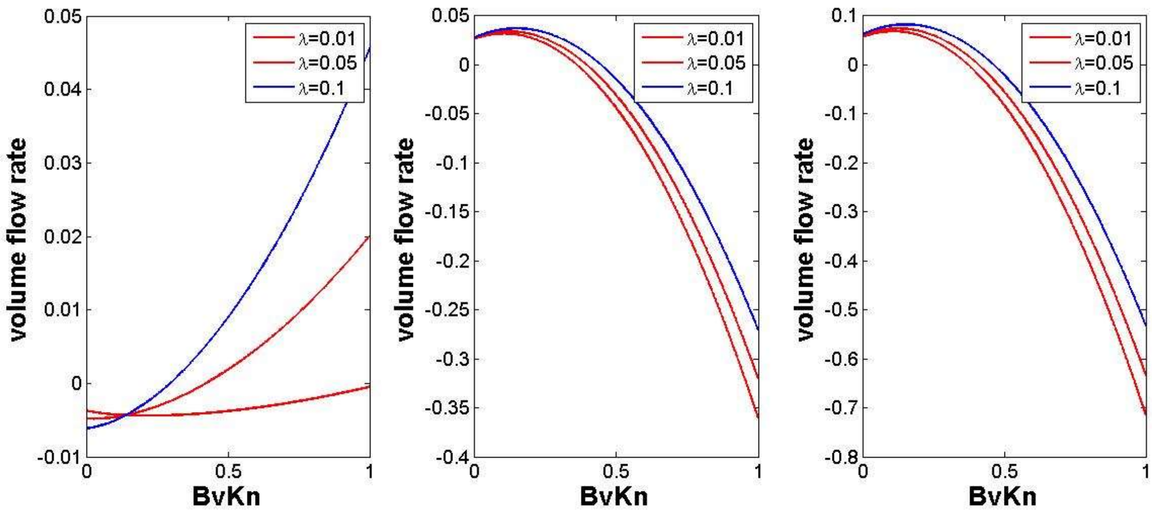

Figure 7: Volume flow rate for λ at (a) ξ=-1, (b) ξ=0 and (c) ξ=1

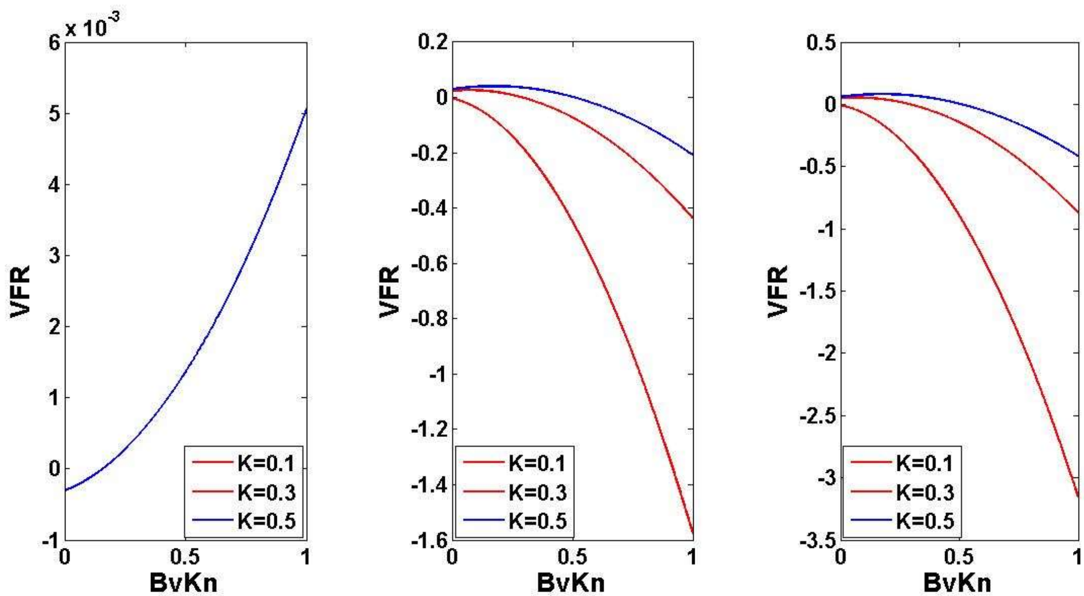

Figure 8: Volume flow rate for Ka at (a) ξ=-1, (b) ξ=0 and (c) ξ=1

ISSN: 1597 – 9928. Science and Education Development Inst., Nigeria

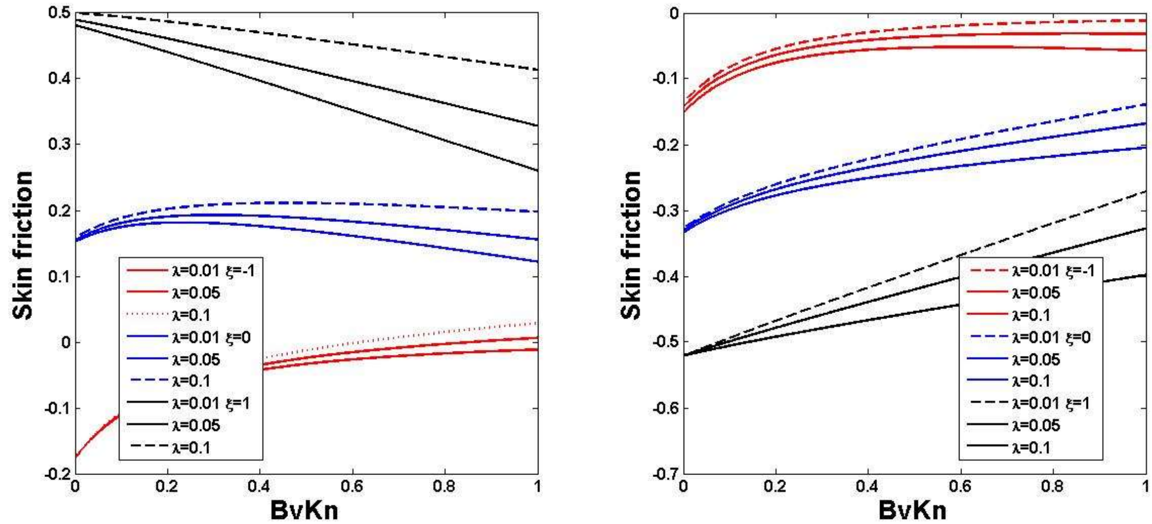

Figure 9: Skin friction versus $\beta_v Kn$ for various values of λ and ξ at (a) y =0 and (b) y=1

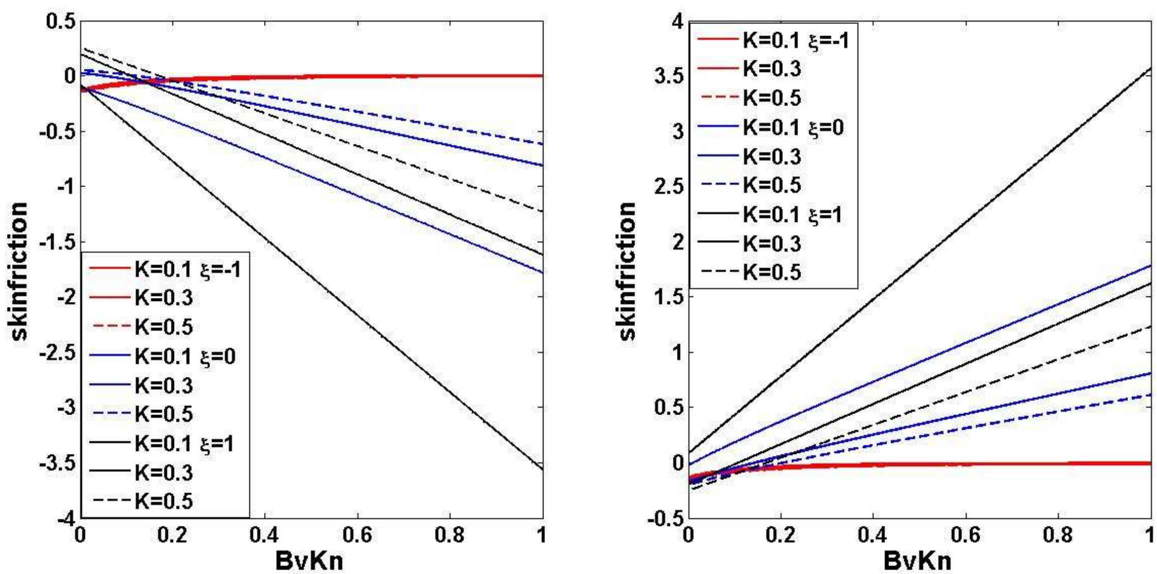

Figure 10: Skin friction versus $\beta_v Kn$ for various values of Ka and ξ at (a) y =0 and (b) y=1

Conclusion

The analysis of a fully developed free convection flow of a chemically reactive, viscous and electrically conducting fluid in a micro-channel embedded with porous material was performed using HPM. Closed form expressions were used to estimate temperature, velocity, volume flow, frictional force and heat transfer rate. The effects of controlling factors such as (λ), ($\beta_v Kn$), (Ka) and (ξ) parameters were estimated, and the results were detailed using line graphs. The current study's noteworthy findings are summarized below:

i. It has been discovered that an increase in fluid acceleration and volume flow rate is observed as (λ), (Ka) and ($\beta_v Kn$) increases for growing values of (ξ).

ii. Similarly, higher levels of (λ) and ($\beta_v Kn$) improve the temperature profile significantly for growing values of (ξ).

iii. Volume flow rate is seen to be strengthen as (λ) and (Ka) are increased for growing levels of (ξ).

iv. As (λ) and (Ka) are increased, the frictional force effect grows at y = 0, while it diminishes at y = 1.

Validation

To validate the accuracy of this present work, we compute a numerical comparison between Jha et al. (2014a) and the current work. Tables 1 and 2 show that there was excellent agreement for the velocity and volume flow rate at both the cold and hot plates. The precision of the current solution, which employs three HPM terms, validates the technique's rapid convergence, demonstrating that the HPM is a useful tool for solving nonlinear systems of differential equations.

Table 1: Shows numerical computations of comparison between the work of Jha et al. (2014a) with the present work for velocity profile for different $\xi = -1, 0, 1$ at $\beta_v Kn$ =0.05, In=1.667, M=1 and taking Ka=1000 as λ approaches 0.

Y	**Jha et al. (2014a) U(Y)**			**Present work U(Y)**		
	$\xi = -1$	$\xi = 0$	$\xi = 1$	$\xi = -1$	$\xi = 0$	$\xi = 1$
0.1	0.0068	0.0156	0.0244	0.0069	0.0157	0.0244
0.2	0.0067	0.0153	0.0239	0.0067	0.0154	0.0240
0.3	0.0066	0.0150	0.0235	0.0066	0.0151	0.0235
0.4	0.0065	0.0148	0.0230	0.0065	0.0148	0.0231
0.5	0.0063	0.0145	0.0226	0.0064	0.0145	0.0226

Table 2: Shows numerical computations of comparison between the work of Jha et al. (2014a) with the present work for volume flow rate for different $\xi = 0 \quad and \quad 1$ at $\beta_v Kn$ =0.0, 0.05 and 0.1, In=1.667, M=1 and taking ka=1000 as λ approaches 0.

$\beta_v Kn$	**Jha et al. (2014a) Q_m**		**Present work Q_m**	
	$\xi = 0$	$\xi = 1$	$\xi = 0$	$\xi = 1$
0.0	0.0379	0.0758	0.0378	0.0755
0.05	0.0479	0.0958	0.0478	0.0957
0.1	0.0575	0.1150	0.0573	0.1148

Conflict of interest
All the authors have declared that there exist no competing interests amongst them

References

Ahmad K. S. and Jha B. K., (2015). Computational methods of transient/steady natural convection flow of reactive viscous fluid in vertical porous pipe, *Asian J. Math. Comput. Res.*, vol. **2,** pp. 74–92.

Alam N, Poddar S.,.Karim M. E, Hasan M. S. and Lorenzini G. (2021). Transient MHD radiative fluid flow over an inclined porous plate with thermal and mass diffusion: an EFDM numerical approach. *Int. Info. Eng. Tech. Assoc.,* **8**(5), 739-749.

Al-Nimr, M. A. and Khadrawi, A. F. (2004). Thermal behavior of a stagnant gas confined in a horizontal microchannel as described by the dual-phase-lag heat conduction model. *Int. J. Thermophy,* vol. **25**, no. 2, pp. 1953–1964.

Ali, F. Samiulhaq, I. K, Mustapha, N and Shafie, S (2012). Unsteady Magnetohydrodynamic Oscillatory Flow of Viscoelastic Fluids in a Porous Channel with Heat and Mass Transfer, *J. Phys. Soc. Japan,*vol. **81**, 064402.

Ayati Z. and Biazar J. (2015). On the convergence of Homotopy Perturbation Method. *J. Egyptian Math Soc.* vol. **23**, pp. 424-428.

Aziz A. and Shams M. (2020). Entropy generation in MHD Maxwell nanofluid flow with variable thermal conductivity, thermal radiation, slip conditions, and heat source. AIP Adv., vol. **10,** 015038, 2020.

Buonomo B and Manca O. (2012). Natural Convection Flow in a Vertical Micro-Channel with Heated at Uniform Heat Flux, *Int.J.Therm.Sci.* vol. **49,** pp. 1333-1344.

Chamkha A, Gorla R.S.R., and Ghodeswar K, (2011). Non-similar solution for natural convective boundary layer flow over a sphere embedded in a porous medium saturated with a nanofluid, *Transp Porous Media,* **86**(1):13–22.

Chamkha A. J., (2007). Mixed convection flow along a vertical permeable plate embedded in a porous medium in the presence of a transverse magnetic field," Numerical Heat Transfer, Part A: Applications: *An International Journal of Computation and Methodology*, **34**(1): 93–103.

Chen C. K and Weng H. C (2005). Natural convection in a vertical micro-channel. *J. Heat Transf.* vol. **127**, pp. 1053-1056.

Frank-Kamenetskii D. A. (1969). Diffusion and Heat Transfer in Chemical Kinetics, Plenum Press, New York.

Gireesha B. J. and S. Sindhu, (2020). MHD natural convection flow of casson fluid in an annular microchannel containing porous medium with heat generation/absorption. *Nonlinear Engineering*, **9**:223-232.

Gul T., Ullah K, Bilal M., Alghamdi W., Asjad M. I. and Abdeljawad T. (2021). Hybrid nanofluid flow within the conical gap between the cone and the surface of a rotating disk, *Sci. Rep.* vol. **11**, pp. 11-18.

ISSN: 1597 – 9928. Science and Education Development Inst., Nigeria

Guriviréddy P., Raju, M. C., Mamatha, B. and Varma, S. K. (2016). Thermal diffusion effect on MHD heat and mass transfer flow past a semi-infinite moving vertical porous plate with generation and chemical reaction. *Appl. Math.* vol. **7** no. 7, pp. 638.

Hamza M M. (2016). Free convection slip flow of an exothermic fluid in a convectively heated vertical channel, *Ain Shams Engineering Journal*, http://dx.doi.org/10.1016/j.asej.2016.08.011

Hamza M. M., Ojemeri G. and Abdulsalam S. (2019). Mixed convection flow of viscous reactive fluids with thermal diffusion and radial magnetic field in a vertical porous annulus. *Comput. Math. Mod.* vol. **30**, no. 3, 2019. DOI:10.1007/510598-019-09451-0

Hamza, M. M. Ojemeri G. and Ahmad, S. K., (2023). Theoretical study of Arrhenius-controlled heat transfer flow on natural convection affected by an induced magnetic field in a microchannel, *Engineering Reports, Wiley*, DOI:10.1002/eng2.12642

Jha B. K., Babatunde Aina and Ajiya A. T. (2014a). MHD natural convection flow in a vertical parallel plate microchannel, *Ain shams Eng.J.* vol. **6**, pp. 289-295.

Jha, B. K., Babatunde Aina and S. B. (2014b). Joseph, Natural Convection Flow in vertical Micro-channel with Suction/Injection, *J. Proc. Mech. Eng*., vol. **228**, no. 3, pp. 171-180.

Jha B. K, SamailaA. K., and AjibadeA. O. (2011b). Transient free-convective flow of reactive viscous fluid in a vertical tube, *Int. Commun. Heat Mass Transf.*, vol. **54,** pp. 2880–2888.

Jha B. K. and Babatunde Aina, (2016). Role of induced magnetic field on MHD natural convection flow in vertical microchannel formed by two electrically non-conducting infinite vertical parallel plates. *Alexandria Eng. J.* vol. **55**, no. 2, pp. 2087-2097.

Jha B. K. and Malgwi, P. B. (2019a). Hall current and ion – slip effects on free convection flow in a vertical microchannel with induced magnetic field. *Heat Transf. Asian Res.* Vol. **48**, no. 8, pp. 1 – 19.

Jha B. K., A. K. Samaila, and A. O. Ajibade (2011a). Transient free-convective flow of reactive viscous fluid in a vertical channel, *Int. Commun. Heat Mass Transf, E*, vol. **38**, pp. 633–637.

Jha, B. K. and Aina, Babatunde, (2015). Mathematical modelling and exact solution of steady fully developed mixed convection flow in a vertical micro-porous-annulus. *J. Afrika Matem-atika*, vol. **26**, pp. 1199-1213.

Jha, B. K., Aina, B and Isa S. (2015). Fully developed MHD natural convection flow in a vertical annular microchannel: an exact solution. *J. King Saudi Univ, Sci.* vol. **27,** pp. 253-259.

Jha, B. K., Malgwi, P. B. and Aina, B. (2017). Hall effects on MHD natural convection flow in a vertical microchannel. *Alexandria Eng. J,* 2017. http://dx.doi.org/10.1016/j.aej.2017.01.038

Joshi Y. and Gebhart B. (1985). Mixed convection in porous media adjacent to a vertical uniform heat flux surface, *Int J Heat Mass Transf,* **28** (9):1783– 1786.

Mahmoudi Y, Hooman K and Vafai K, (2020). Convective Heat Transfer in Porous Media (New York, USA: Taylor & Francis Group, LLC CRC Press)

Makinde O. D. (2008). Thermal criticality in viscous reactive flows through channels with a sliding wall: an exploitation of the Hermite– Pade approximation method, *J. Math. Comput. Model*, vol. **47**, pp. 312–317.

Muthuraj R. and Srinivas S. (2010). Mixed convective heat and mass transfer in a vertical wavy channel with travelling thermal waves and porous medium, *J. Comput. Math. Appl.,* vol. **59**, pp. 3516–3528.

Ojemeri G., Hamza M. M. (2022). Heat transfer analysis of arrhenius-controlled free convective hydromagnetic flow with heat generation/absorption effect in a micro-channel, Alexandria Eng. J, vol **61**, pp 12797-12811.

Ojemeri G., Omokhuale E., Hamza M. M., Onwubuya I. O. and Shuaibu A. (2023). A Computational Analysis on Steady MHD Casson Fluid Flow Across a Vertical Porous Channel Affected by Thermal Radiation Effect. International Journal of Science for Global Sustainability, vol. 9(1), https://doi.org/ 10.57233/ijsgs.v9i1.393

Ojemeri, G., Onwubuya I. O.,and Abdulsalam S. (2019). Effects of Soret and Radial magnetic field of a free convection slip flow in a viscous reactive fluid towards a vertical porous cylinder. *Cont. J. Applied Sci,* vol. **14,** no. 1, pp. 25-45. DOI: 10.5281/zenodo.265200.

Saeed A. and Gul T. (2021). Bio-convection casson nanofluid flow together with Darcy-Forchheimer due to a rotating disk with thermal radiation and Arrhenius activation energy, *SN Appl. Sci*. vol. **3**, pp. 78.

Sheikholeslamia M. and Gorji-Bandpy M. (2014). Free Convection of Ferro-fluid in a Cavity Heated from below in the Presence of an External Magnetic Field, *Powd. Tech.* vol. 256, pp. 490–8.

Weng, H. C., Chen, C. K. (2009). Drag reduction and heat transfer enhancement over a heated wall of a vertical annular microchannel, *Int. J. Heat Mass Transf,* vol. **52,** pp. 1075–1079, 2009.

Appendix

$$A_0 = \xi + \frac{BnKnIn(1-\xi)}{1+2BnKnIn}, \qquad A_1 = \frac{(1-\xi)}{1+2BnKnIn}, \qquad A_2 = BnKnInA_3$$

$$A_3 = \frac{\lambda BnKnIn(c_4 - c_5 + c_6) + \lambda(c_1 - c_2 + c_3)}{1+2BnKnIn}, \quad A_4 = BnKnInA_5,$$

$$A_3 = \frac{\begin{array}{l} -BnKnIn(-c_{20} + c_{21} - c_{22} - c_{23} + c_{24} - c_{25} + c_{26} - c_{27} + c_{28} - c_{29} + c_{30} + c_{31}) \\ +\lambda(4\lambda - 2e\lambda)(c_8 - c_9 + c_{10}) + c_{11}(4\lambda - 2e\lambda)(c_{12} - c_{13} + c_{14}) + c_{15}(4\lambda - 2e\lambda) \\ -\lambda^2(c_{16} - c_{17} + c_{18}) - c_{19} \end{array}}{1+2BnKnIn}$$

$$D_2 = BnKnD_3, \; D_3 = \frac{BnKnA_0 + BnKn\frac{A_1}{2} + \frac{A_0}{2} + \frac{A_1}{6}}{(1+2BnKn)}$$

$$D_4 = BnKnD_5, \; D_5 = \frac{-BnKnc_{35} - \lambda BnKn(c_{36} - c_{37} + c_{38}) - BnKnc_{39} - c_{30} - c_{34} - \lambda(c_{31} + c_{32} + c_{34})}{(1+2BnKn)}$$

$$c_1 = \frac{1}{2} + \frac{A_0}{2} + \frac{A_1}{2}, \qquad c_2 = e(\frac{A_0^2}{2} + \frac{A_0A_1}{3} + \frac{A_1^2}{12}), \qquad c_3 = 2(\frac{A_0^2}{2} + \frac{A_0A_1}{3} + \frac{A_1^2}{12})$$

$$c_4 = 1 + A_0 + \frac{A_1}{2}, \qquad c_5 = e(A_0^2 + A_0A_1 + \frac{A_1^2}{3}), \qquad c_6 = 2(A_0^2 + A_0A_1 + \frac{A_1^2}{3}),$$

$$c_8 = \frac{A_0}{24} + \frac{A_0^2}{24} + \frac{A_0A_1}{120}, \quad c_9 = e(\frac{A_0^3}{24} + \frac{A_0^2A_1}{60} + \frac{A_0A_1^2}{360}), \qquad c_{10} = 2(\frac{A_0^3}{24} + \frac{A_0^2A_1}{60} + \frac{A_0A_1^2}{360}),$$

$$c_{11} = \frac{A_0A_3}{6} + \frac{A_0A_2}{2}, \qquad c_{12} = (\frac{A_1}{40} + \frac{A_0A_1}{40} + \frac{A_1^2}{180}), \qquad c_{13} = e(\frac{A_0^2A_1}{40} + \frac{A_1^2A_0}{60} + \frac{A_1^3}{504}),$$

$$c_{14} = 2(\frac{A_0^2A_1}{40} + \frac{A_1^2A_0}{60} + \frac{A_1^3}{504}), \quad c_{15} = \frac{A_1A_3}{12} + \frac{A_1A_2}{6}, \qquad c_{16} = \frac{1}{24} + \frac{A_0}{24} + \frac{A_1}{120},$$

$$c_{17} = e(\frac{A_0^2}{24} + \frac{A_0A_1}{60} + \frac{A_1^2}{360}), \qquad c_{18} = 2(\frac{A_0^2}{24} + \frac{A_0A_1}{60} + \frac{A_1^2}{360}), \qquad c_{19} = \lambda(\frac{A_3}{6} + \frac{A_2}{2}),$$

$$c_{20} = \frac{A_0}{6} + \frac{A_0^2}{6} + \frac{A_0A_1}{24}, \; c_{21} = e\lambda(4\lambda - 2e\lambda)(\frac{A_0^3}{6} + \frac{A_0^2A_1}{12} + \frac{A_0A_1^2}{60}),$$

$$c_{22} = 2\lambda(4\lambda - 2e\lambda)(\frac{A_0^3}{6} + \frac{A_0^2A_1}{12} + \frac{A_0A_1^2}{60}), \qquad c_{23} = (4\lambda - 2e\lambda)(\frac{A_0A_3}{2} + A_0A_2),$$

$c_{24}=\lambda(\frac{A_1}{8}+\frac{A_0A_1}{8}+\frac{A_1^2}{30}),\qquad c_{25}=e\lambda(4\lambda-2e\lambda)(\frac{A_0^2A_1}{8}+\frac{A_1^2A_0}{15}+\frac{A_1^3}{72}),$

$c_{26}=2\lambda(4\lambda-2e\lambda)(\frac{A_0^2A_1}{8}+\frac{A_1^2A_0}{15}+\frac{A_1^3}{72}),\qquad c_{27}=(4\lambda-2e\lambda)(\frac{A_1A_3}{3}+\frac{A_1A_2}{2}),$

$c_{28}=\lambda^2(\frac{1}{6}+\frac{A_0}{6}+\frac{A_1}{24}),\ c_{29}=e\lambda^2(\frac{A_0^2}{6}+\frac{A_1A_0}{12}+\frac{A_1^2}{60}),\qquad c_{29}=2\lambda^2(\frac{A_0^2}{6}+\frac{A_1A_0}{12}+\frac{A_1^2}{60}),$

$c_{31}=\lambda(\frac{A_3}{2}+A_2),\qquad c_{32}=-\frac{A_0}{24}-\frac{A_1}{120}+\frac{D_3}{6}+\frac{D_2}{2},\qquad c_{33}=\frac{1}{24}+\frac{A_0}{24}+\frac{A_1}{120},$

$c_{34}=e(\frac{A_0^2}{24}+\frac{A_0A_1}{60}+\frac{A_1^2}{360}),\qquad c_{35}=2(\frac{A_0^2}{24}+\frac{A_0A_1}{60}+\frac{A_1^2}{360}),\qquad c_{36}=-\frac{A_3}{6}-\frac{A_2}{2},$

$c_{37}=(M^2+\frac{1}{K})\left(-\frac{A_0}{6}-\frac{A_1}{24}+\frac{D_3}{2}+D_2\right),\qquad c_{38}=\frac{1}{6}+\frac{A_0}{6}+\frac{A_1}{24}),\qquad c_{39}=e(\frac{A_0^2}{6}+\frac{A_1A_0}{12}+\frac{A_1^2}{60}),$

$c_{40}=2(\frac{A_0^2}{6}+\frac{A_1A_0}{12}+\frac{A_1^2}{60}),\qquad c_{41}=-\frac{A_3}{2}-A_2$